Received: 14 February 2024 | Accepted: 9 November 2024

DOI: 10.1111/mice.13384

INDUSTRIAL APPLICATION

COMPUTER-AIDED CIVIL AND INFRASTRUCTURE ENGINEERING

WILEY

A bridge point cloud databank for digital bridge understanding

Hongwei Zhang | **Yanjie Zhu** | **Wen Xiong** | **C. S. Cai**

Department of Bridge Engineering, School of Transportation, Southeast University, Nanjing, China

Correspondence
Wen Xiong and Yanjie Zhu, Department of Bridge Engineering, School of Transportation, Southeast University, Nanjing 211189, China.
Email: wxiong12@hotmail.com; wxiong@seu.edu.cn and yanjie@seu.edu.cn

Funding information
National Natural Science Foundation of China, Grant/Award Numbers: 52378135, 52108118

Abstract

Despite progress in automated bridge point cloud segmentation based on deep learning, challenges persist. For instance, the absence of a public point cloud dataset specifically designed for bridge instances, and the existing bridge point cloud datasets display a lack of diversity in bridge types and inconsistency in component labeling. These factors may hinder the further improvement of accuracy in bridge point cloud segmentation. In this paper, a universal multi-type bridge point cloud databank, named BrPCD, consisting of a total of 98 point cloud data (PCD; 10 of them are obtained from scanning, and the rest is obtained by data augmentation) from small to long-span bridges, is established. Additionally, a method for augmenting bridge PCD is proposed, significantly enriching the spatial feature information of bridges within the dataset. Furthermore, based on the introduced data annotation rules, a uniform categorization of semantic labels for bridge components is implemented, enhancing the applicability of our dataset across various semantic segmentation tasks for different types of bridges. A benchmark testing was conducted on the BrPCD using the PointNet model. The segmentation results indicate that the parameters learned through the BrPCD enable accurate segmentation at the level of various types of bridge components. In other words, the BrPCD can function as a universal dataset, applicable for testing various networks aimed at bridge point cloud segmentation.

1 | INTRODUCTION

In recent years, the building information model, owing to its robust digital data storage capability, has gradually demonstrated its advantages in providing engineers with critical information in construction (Z. Zhang et al., 2024), health monitoring (Javadinasab et al., 2021; Pezeshki, Adeli, et al., 2023), and digital model analysis (Y. Zhang et al., 2024). With the emergence of 3D laser scanning technology, engineering structures including bridges have gained new avenues for digitization and modeling. As an essential technique and key component in establishing bridge information models, 3D laser scanning technology represents bridge structures as point cloud data (PCD) in three-dimensional space. Engineers detect independent labeled point clouds of bridge components within the PCD and generate geometric models based on these segmented individual component point clouds and their spatial relationships. Simultaneously, researchers working with PCD can directly extract precise spatial characteristics of the

majority of bridge components within the point cloud of the bridge.

However, efficiently and accurately assigning semantic labels to different bridge components within the entire bridge PCD, that is, achieving point cloud semantic segmentation, is a crucial step for both (Bridge Information Modeling) BrIM and some point cloud-based bridge shape detection tasks. Point cloud semantic segmentation is a fundamental technique in PCD processing, aiming to transform raw 3D PCD into highlighted independent regions. The earliest method used for point cloud segmentation was manual point cloud segmentation using the selection function of point cloud processing software. However, this approach is impractical for complex bridge segmentation tasks due to the extensive time required and the potential for classification errors during the human-operated process. To reduce the manual cost of segmentation, several algorithms have been developed that leverage the inherent spatial characteristics of bridges, along with bridge design knowledge. These methods have proven effective for bridges with specific structures. To further enhance segmentation efficiency and overcome the limitations posed by specific bridge forms, deep learning techniques have been applied to bridge point cloud semantic segmentation, yielding promising results. This approach uses parameters learned from training data to perform semantic predictions on unknown data, thereby providing semantic information to raw point clouds with a high degree of automation. The training process of deep learning requires a dataset with sufficient samples to provide the network with comprehensive spatial feature information. However, the collection of bridge point clouds is often time-consuming, and the completeness of the data can be challenging to ensure. These factors may limit the development of bridge point cloud semantic segmentation research based on deep learning.

In this paper, a multi-type bridge point cloud databank named BrPCD is introduced, which addresses the deficiency in existing research datasets and provides a unified resource for bridge point cloud segmentation tasks. Moreover, the proposed BrPCD can also support the research efforts on methods development, such as the comparative assessment and cross-evaluation of various potential segmentation methods.

The differences in both the quantity and features of the point clouds in the dataset can lead to variations in the outcomes of model training. For the task of bridge component recognition based on deep learning, a practically valuable point cloud dataset should be established as a collection containing various types of bridge point clouds, and the number of bridges included should be sufficient to meet learning requirements. At the same time, the semantic labels in the dataset should effectively encompass component features and have general applicability across different bridge segmentation models.

Based on these principles, our proposed BrPCD encompasses multiple types of bridges, offering a substantial collection of both real-measured and synthetically generated bridge PCD. Real bridge data serve as the foundation for BrPCD. This paper conducted field measurements or collected PCD from several distinct real bridges, including the most common types found in engineering, such as continuous girder bridges and simply supported beam bridges. Furthermore, the BrPCD also includes a collection of long-span bridges, including cable-stayed bridges and suspension bridges. In addition to real bridge PCD, this paper proposes a data augmentation method to generate a large volume of PCD with diverse features. This augmentation significantly enhances the dataset's richness in terms of bridge feature information.

In addition to PCD, the labels in the dataset are another element, reflecting the various point cloud semantic features contained within it and determining the dataset's application scenarios. The BrPCD employs a unified method for classifying bridge components. Labels are categorized solely based on the spatial features of components rather than their affiliation with a specific bridge type. The label categories include girder, deck, pier, main cable, suspender, and stay, considering these as crucial component-level objects in the digitalization process of bridges. This classification method follows the principle of feature induction, which could enhance the accuracy of segmentation networks. All bridge point clouds in the BrPCD have been annotated at the component level according to the aforementioned classification scheme.

To validate the effectiveness of BrPCD, this paper conducted segmentation tasks using PointNet, a direct point cloud segmentation network. Despite the development of numerous models that outperform PointNet in terms of accuracy, PointNet was selected for its simplicity and suitability for validating the effectiveness of large-scale point cloud datasets. Additionally, using PointNet for benchmark testing on bridges allows for a more intuitive assessment of the original performance of direct segmentation networks in bridge point cloud segmentation tasks. This provides clearer references for the subsequent development of networks that are more suitable for bridge point cloud segmentation. Therefore, PointNet was chosen as the testing network for the BrPCD in this study.

The rest of this paper is organized as follows: Section 2 discusses the current research. The creation process of the BrPCD is presented in Section 3. Subsequently, Section 4 showcases the statistical overview of bridge point cloud types within the BrPCD. The validation process of the BrPCD and the analysis of bridge point cloud

segmentation results are presented in Section 5. Finally, Section 6 concludes the paper.

2 | RELATED WORK

To address the inefficiency and potential for human–machine interaction errors in the manual point cloud segmentation, researchers have integrated point cloud processing algorithms with contextual information to achieve automated semantic segmentation of point clouds. One approach, known as a bottom-up segmentation algorithm, aims to extract the point cloud's raw geometric features to a more abstract level for segmentation (Laefer and Linh, 2017; G. Zhang et al., 2015). This method divides the point cloud into different clusters and classifies them according to engineering knowledge and experience. Another point cloud segmentation algorithm, referred to as a top-down segmentation method, utilizes the point cloud's geometric features and prior design knowledge as references (Belsky et al., 2016; Ma et al., 2018). Both algorithms leverage the inherent geometric features of point clouds to achieve segmentation for different objects.

Several studies have validated the feasibility of the aforementioned algorithms based on different principles for bridge point cloud segmentation. Riveiro et al. (2016) achieved component segmentation of a stone bridge using point cloud surface normal histograms. Lu et al. (2019) classified various components of existing reinforced concrete girder bridges using a slicing algorithm. These studies successfully implemented segmentation on their respective bridge point cloud datasets using the proposed algorithms. Nevertheless, current techniques—whether utilizing a top-down or bottom-up algorithm—are limited to certain types of bridges and cannot be tailored to semantic point cloud segmentation for other bridge kinds.

To transcend the limitations of bridge types, certain studies have begun to explore deep learning-based networks (Hinton and Salakkhutdinov, 2006; LeCun et al., 2015) for point cloud segmentation. With this method, features of training samples are learned across several dimensions using deep neural networks, and then the learned parameters are used to predict unknown data.

Learning-based methods have also been applied in recommendation systems (Martins et al., 2020), point cloud completion (Matono et al., 2024), high-rise building damage detection (Rafiei and Adeli, 2017), building response prediction (Perez-Ramirez et al., 2019), and real-time structural vibration measurement (Pan et al., 2023). Kalogerakis et al. (2010) pioneered the concept of learning for training labeled 3D datasets, utilizing the feature extraction capabilities of networks to achieve point cloud classification. Based on the processing approach of PCD, deep learning-based point cloud segmentation can be classified into indirect and direct methods (R. Zhang et al., 2021). Indirect semantic segmentation methods initially transform irregular PCD into structured formats such as 3D voxels (L. Wang et al., 2018; Xu et al., 2018) or multi-view representations (Boulch et al., 2018; Q. Liang et al., 2020) and then employ conventional networks like convolutional networks for point cloud semantic segmentation (J. Zhang et al., 2019).

This indirect transformation process can lead to information loss in the point cloud and also reduce data processing efficiency. To avoid these issues, direct point cloud segmentation methods have been developed. Within the realm of direct segmentation methods, PointNet (Qi, Su, et al., 2017) stands as the earliest and pioneering approach. It can take each point in a point cloud as input, extract independent features for each point through multi-layer perceptrons (MLPs) in different dimensions, aggregate these features into global point cloud features, incorporate the T-Net network architecture for rotational invariance, and ultimately output semantic labels for each point. While serving as an initial attempt in the realm of direct point cloud segmentation methods, the PointNet, despite being capable of achieving point cloud segmentation in specific scenarios, often struggles due to its limited capacity to extract local features from point clouds. This limitation hampers PointNet's ability to effectively perform advanced segmentation tasks at a higher level. Subsequent research has optimized the network using various approaches to achieve higher segmentation accuracy. PointNet++ (Qi, Yi, et al., 2017) maintains the framework structure of PointNet while learning point cloud features in a hierarchical manner. Each layer consists of sampling, grouping, and feature extraction components, addressing the issue of limited local feature extraction capability in PointNet. However, both networks still fail to fully consider the interaction between neighboring points, resulting in limited classification ability for fine-grained point clouds. Inspired by the layered structure of PointNet++, researchers have proposed networks such as PointWeb (Zhao et al., 2019), Momenet (Joseph-Rivlin et al., 2019), RandLA-Net (Hu et al., 2020). These networks employ different feature capture methods to more efficiently retain local point cloud features while improving computational and storage efficiency.

Some scholars have attempted to treat point clouds as graph structures within the direct point cloud segmentation networks. Graph neural network (GNN) is a type of neural network that operates on graph structures and relies on information propagation between nodes in the graph to capture features. The concept was initially introduced by Gori et al. (2005) and further refined by Scarselli et al. (2009). Kipf and Welling (2017) introduced

convolutional operations on top of GNN, formally introducing the concept of graph convolutional neural network (GCNN). GCNN was first utilized for feature extraction in structured data such as images and performed well in semi-supervised classification tasks. Simonovsky and Komodakis (2017) developed an edge-conditioned convolutional (ECC) neural network that can be applied to PCD. This network treats the points in a point cloud as vertices in a graph structure and aggregates vertex feature information using max-pooling sampling. However, since point clouds are non-structured data, ECC requires converting the point cloud into a graph structure for graph convolution computations, which consumes significant computational resources and leads to suboptimal segmentation results. Based on ECC, a dynamic GCNN called DGCNN was proposed (Y. Wang et al., 2019). This network constructs a local neighborhood graph with a fixed number of edge nodes and then utilizes the EdgeConv module to extract edge vectors between the central point and the edge nodes, ultimately aggregating them into local point cloud features. EdgeConv takes into account the distance between edge nodes and the central point but neglects the direction of the vectors, resulting in the loss of some local features. Subsequent research has focused on exploring the potential of graph convolutional networks in point cloud segmentation. These studies have introduced different modules and structures to enhance the connections between neighboring target nodes.

In addition to that, many researchers have achieved point cloud segmentation using different deep neural network structures. For example, methods based on recurrent neural networks (Himmelsbach et al., 2010), attention mechanisms (J. Yang et al., 2019), and material augmented (H. Liang et al., 2024) have been explored, as well as approaches that combine instance segmentation. These methods can be considered as inheriting the idea of directly processing point clouds from PointNet and integrating principles from various popular networks in the field of machine learning. As a result, they have achieved higher accuracy in point cloud segmentation (Chen and Cho, 2022).

As indicated, the growing significance of deep learning methods can be observed in the field of point cloud segmentation (Martens et al., 2023). It is widely acknowledged that deep semantic segmentation networks require extensive 3D object datasets for training and validation to assess their segmentation performance in various scenarios. Researchers use these segmentation results to purposefully refine the networks, ultimately obtaining output parameters that meet the task requirements. With the increasing emergence of deep neural networks for point clouds, the demand for large-scale point cloud datasets from various scenes has also grown significantly. In recent years, multiple datasets have been released for the performance evaluation of various deep learning algorithms for point cloud processing tasks, including classification, segmentation, and detection. These datasets can be divided into indoor and outdoor datasets based on different scenarios. ModelNet (Wu et al., 2015), ShapeNet (Yi et al., 2017), S3DIS (Armeni et al., 2016), UWA Dataset (Mian et al., 2006), and PartNet (Mo et al., 2019) are common indoor 3D point cloud datasets. They contain PCD of a large number of indoor objects with instance-level annotations, including everyday objects such as tables, chairs, computers, sofas, ceilings, and walls. Instance-level annotations are provided for all categories. Some studies focus on fine-grained 3D object segmentation, further subdividing shapes and meshes based on instance segmentation. Widely used outdoor datasets include VKitti (Gaidon et al., 2016), Semantic3D (Hackel et al., 2018), and Apollo (Song et al., 2019), which include larger-scale outdoor scenes such as roads, buildings, and squares. Noichl (2024) proposed a synthesizing method for industrial plants. These indoor and outdoor point cloud datasets provide a comprehensive platform for improving the accuracy and performance iteration of various point cloud semantic segmentation algorithms, promoting the advancement of these algorithms in replacing human understanding of different 3D scenes.

Some scholars have recognized the potential of deep learning networks for bridge point cloud segmentation and have trained and validated segmentation networks using small amounts of measured bridge PCD as datasets. The majority of studies in bridge point cloud segmentation have focused on utilizing direct methods, which involve taking the individual points within the point cloud as input. Through the feature extraction capabilities of neural networks, these studies achieve semantic segmentation results for the targeted objects. Kim et al. conducted point cloud scans of seven small-span girder bridges, with a maximum span of 38 m (Hyunjun Kim et al., 2020). They employed the early direct segmentation model PointNet, using four bridges for training and three bridges for testing, achieving segmentation accuracy of over 80%. However, higher prediction errors were observed at the connections between components. Another study by Kim et al. involved scanning three different types of girder bridge point clouds (Hyeonsoo Kim et al., 2020). The point clouds were divided into left and right parts along the longitudinal direction of the bridges, and three-fold cross-validation was performed to create training and testing datasets. The researchers trained and tested three popular deep segmentation networks, namely, PointNet, DGCNN, and PointCNN. The results indicated that DGCNN achieved the highest prediction accuracy when the overlap ratio of training blocks was set to 80%. However, it exhibited

less accuracy than PointCNN at the connections between bridge piers and the background. Lee proposed a layered deep-learning model based on the DGCNN network (Lee et al., 2021). This network boasted a wider perception range of features, enabling more precise segmentation of towering utility poles on bridges. However, due to the limited number of bridges in the training dataset, the segmentation accuracy of some components is relatively low. Xia et al. (2022) proposed an algorithmic and learning-based method that combines a local descriptor with a fully connected multilayer neural network, achieving high-precision segmentation of bridge point clouds in small-sample conditions. However, this method consists of separate algorithmic and network modules, leading to complexity and low computational efficiency, limiting its applicability.

To address the issue of insufficient training data due to the difficulty of collecting real bridge PCD, some researchers have expanded the training dataset by synthesizing virtual bridge point cloud datasets. These datasets are then used to train the developed networks. X. Yang et al. (2022) introduced a weighted superpoint graph method to address the data imbalance in point clouds before utilizing PointNet and graph networks for bridge point cloud segmentation. Synthetic PCDs were generated based on real bridge Revit files, resulting in significant improvements in segmentation accuracy, compared to PointNet and DGCNN. Jing (2022, 2024) focused on arch bridges and generated numerous different-sized 3D masonry arch bridge models through topological iteration from two original shapes. They proposed BridgeNet (Jing et al., 2022) and a lightweight transformer (Jing et al., 2024) to successfully achieve recognition of the main components of masonry arch bridges. However, the datasets established in both studies are limited to a specific bridge type, and the network segmentation performance has only been validated within a specific range.

The aforementioned studies on bridge point cloud segmentation based on deep neural networks have achieved the goal of automated segmentation of bridge components. Some studies have also attempted to establish synthetic bridge point cloud datasets. However, several independent studies collected PCD from bridges with significant differences in types. Therefore, whether the proposed models can perform well in other types of bridge point cloud segmentation tasks is currently unknown. This is because the lack of a unified model testing platform has prevented the validation of the general applicability of segmentation models in independent studies. Furthermore, the established bridge datasets are limited in terms of bridge types, mainly containing structurally similar medium-span beam bridges or arch bridges. Consequently, these datasets are challenging to use as universal training resources for various types of bridge point cloud segmentation tasks. To the authors' knowledge, generalized multi-type bridge point cloud datasets specially designed for bridges have not been discovered from the current research.

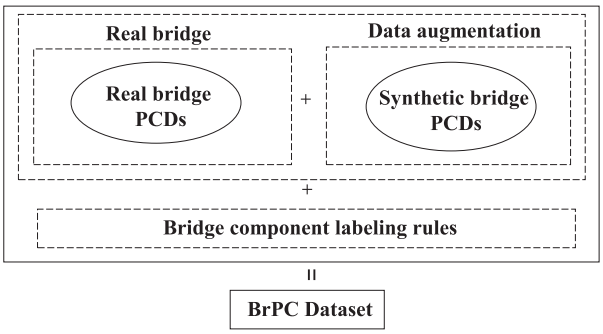

FIGURE 1 Principle of bridge point cloud databank (BrPCD) construction. PCD, point cloud data.

3 | BrPCD CONSTRUCTION

This study aims to establish a bridge point cloud dataset with broad utility to support rapidly developed research of bridge digitalization. The process of constructing BrPCD is indicated in Figure 1. The first step involves collecting a diverse set of real bridge PCD, ensuring that the dataset encompasses a wide range of spatial characteristics of bridges. However, relying solely on real point clouds often proves inadequate in meeting the semantic prediction requirements of diverse and unfamiliar point clouds. Therefore, to enhance the feature diversity within the dataset, a data augmentation method based on real bridge parameters has been proposed. This method is not only used for establishing BrPCD but also provides researchers in the same field with a referenceable method for generating bridge PCD. Last, to ensure the dataset's broad applicability across diverse bridge segmentation networks, a concise and universal semantic label is imperative.

3.1 | PCD collection and clean

The scanning device used in this study is a terrestrial laser scanner, specifically the Leica P50. It offers high precision, with a maximum accuracy of 1.2 mm. The scanner has four distance modes: 120 m, 270 m, 570 m, and 1 km. These modes allow for efficient scanning and enable the capture of relatively complete PCD for various types of bridges.

From the perspective of scanning methods, the survey station positions for different bridge types are similar, with distinctions lying in the parameter settings of the scanners corresponding to different bridge spans. For the scanning

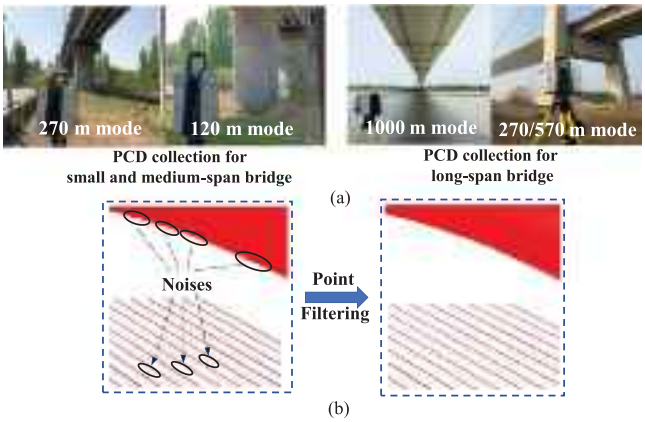

FIGURE 2 (a) Bridge point cloud data (PCD) collection and (b) noise filtering.

of small and medium-span bridges, it is generally necessary to capture PCD from different angles to ensure complete coverage. During scanning, the distance parameter of the scanner is adjusted to 120 or 20 m based on the actual span of the bridge to improve scanning efficiency. It is also important to maintain consistent resolution for multiple scans of the same bridge to ensure similarity in point cloud density across different parts.

Regarding the scanning of bridge towers in long-span bridges, it is typically feasible to set up scanning stations on the ground near the towers. In such cases, the 270 or 540 m mode is generally sufficient to scan the top of the towers, even for the farthest sections. However, when scanning the main girders or main cables, there may be limitations due to geographical constraints, as many long-span bridges are built over rivers. In such scenarios, it is necessary to adjust the distance parameter to be greater than 1 km to capture the PCD of these components to the fullest extent possible. The data acquisition process for bridges with different spans is illustrated in the accompanying Figure 2a.

During the process of obtaining bridge PCD, some noise points may exist near the complete bridge point cloud due to bridge surface characteristics, scanning environment, weather conditions, and instrument errors. Though the number of these noise points is not large, they do not belong to the bridge structure and need to be filtered out to avoid affecting the learning process of the deep neural network and reducing segmentation accuracy. In this paper, a statistical analysis-based point cloud denoising method called statistical outlier removal (SOR) was employed. SOR detects and removes outlier points by analyzing the distribution of each point and its neighboring points in the point cloud. As illustrated in Figure 2, we utilized SOR to filter out noise points near the main girder and cable point clouds to prevent interference with the prediction process. It should be noted that the number of neighboring points, which is a key parameter in SOR, should be set in accordance with the density of the point cloud. This ensures that local features are effectively captured while accurately identifying outliers.

3.2 | Data augmentation for bridge PCD

Training deep learning models often requires a large amount of training data. However, the collection of outdoor bridge PCD is a labor-intensive task. Even for a small and medium-span bridge, it typically takes several hours to complete the scanning process. The complexity of the scanning process limits the availability of manually collected bridge PCD, which may not contain sufficient spatial features to train deep learning models. Hence, this paper presents a bridge PCD augmentation method as shown in Figure 3. First, a method for generating virtual point clouds based on the extraction of feature parameters from point clouds or drawings, along with parameter transformation and cross-section replication, has been proposed to synthesize bridge PCD with diverse morphological characteristics. Additionally, a deficient point cloud generation method is proposed for long-span bridge point clouds, enabling the simulation of the real scanning state of such bridges.

In contrast to existing PCD augmentation methods for bridges, the proposed data augmentation method has the following unique improvements: (1) It is adaptable to the generation of virtual point clouds for most types of bridges. (2) Although the geometric parameters of virtual bridges are modified, they adhere to bridge construction knowledge and thus comply with engineering standards for bridge building. (3) It offers researchers an open framework. Any researcher can utilize their own real bridge point clouds or blueprints to generate virtual point clouds that meet specific requirements using this data augmentation approach.

3.2.1 | Parameter extraction in two situations

Bridge spatial parameters determine the unique morphological features of a bridge and are crucial information required for subsequent virtual point cloud generation. Therefore, obtaining girder cross-sectional dimensions, bridge extension equations, span parameters, and so forth in various situations is a prerequisite for establishing the BrPCD.

Design drawings are available: A sample augmented with data from an acquired point cloud of a specific bridge can be created. If the bridge's design drawings are

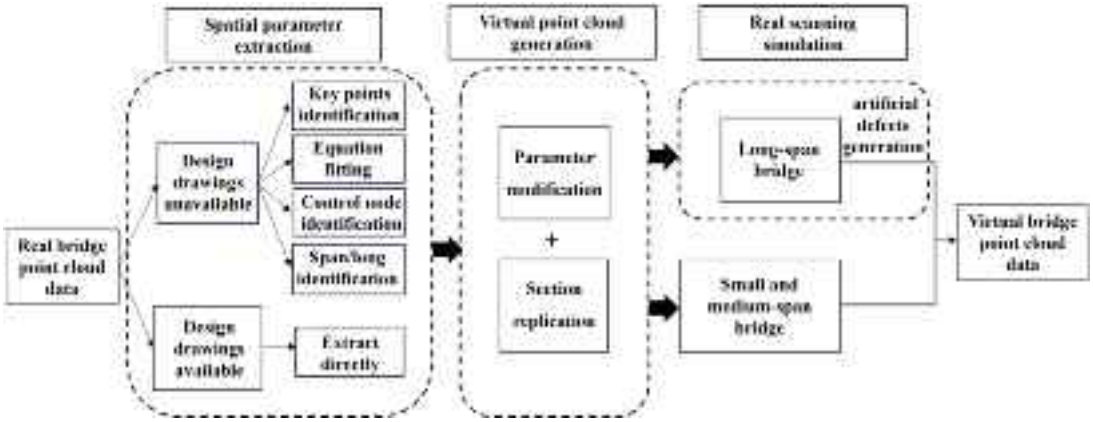

FIGURE 3 Bridge PCD augmentation flow.

available, the bridge's spatial parameters for data augmentation can be directly extracted from the corresponding drawings. The cross-sectional dimensions of the girder can be obtained from the section construction diagrams of the girder, while essential information such as the plan extension equations, longitudinal extension equations, and span can be extracted from the bridge's plan view and elevation drawings.

Design drawings are unavailable: However, in many cases, it may not be possible to access the design drawings of certain bridges due to factors such as their historical age or protected copyrights. To obtain the spatial parameters necessary for data augmentation, this study proposes a straightforward yet practical point cloud-based parameter extraction method. Taking the example of girder elements, the following section outlines the process of extracting spatial parameters for bridge components with spatial extension characteristics. Other components can undergo parameter extraction using the same method based on their spatial characteristics.

1. Girder key points identification. The key points of the girder include spatial coordinates that reflect the bridge's planar and longitudinal extension information. Typically, these key points consist of a sequence of 3D coordinates located at the same lateral positions on the girder. As illustrated in Figure 4, multiple parallel planes are established to segment the bridge point cloud. Considering lateral position consistency and precise localization, along the intersection lines of each plane with the point cloud, the set of intersection points between the bottom plate line and the web line is selected as the target key points.
2. Initial planar/longitudinal extension equation fitting. As shown in Figure 4, all the lateral–longitudinal coordinates of the key points can be used to fit the initial plane equation, denoted as $y = E_P\ (x)$. Simultaneously, all the vertical–longitudinal coordinates of the key points can be used to fit the initial longitudinal equation, denoted as $z = E_L\ (x)$. Based on engineering experience, for the planar equation, if there is a noticeable curvature in the bridge's planar trend, it is recommended to use circular curves or polynomials for fitting (the specific choice should depend on the fitting error). In other cases, linear fitting can be used. For longitudinal equations, polynomial fitting is suitable for small and medium-span variable cross-section bridges, while linear fitting is appropriate for constant cross-section girders. For long-span bridges, circular curves can be utilized for fitting.
3. Girder end section size control node identification. The end sections of the girder define the initial position for the spatial extension of the girder component, and the size control nodes constitute the fundamental morphological information of the section. As illustrated in Figure 4, obtaining the 3D coordinates of each size control node, which are essentially the corner points in the section, provides spatial positional information for creating the primitive point set PS_{pr} in subsequent steps.

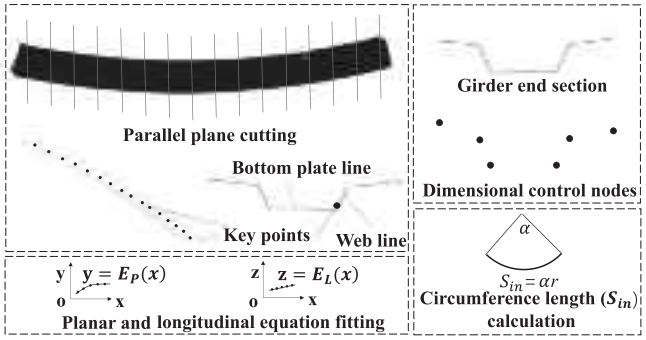

FIGURE 4 Spatial feature extraction based on point cloud.

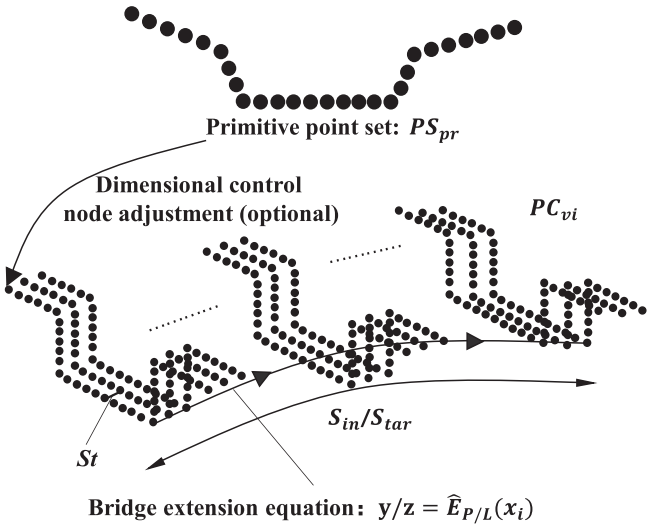

FIGURE 5 Section replication based on primitive point set.

4. Initial span/identification. For straight-line planar girders, the initial span, denoted as S_{in}, can be directly determined by the linear distance between the corresponding nodes at both ends of the girder. In the case of curved planar girders, based on the equation $y = E_P(x)$, as depicted in Figure 4, the initial span S_{in} of the bridge is calculated using the method for measuring the circumference length, where r is the radius of the planar circular curve.

3.2.2 | Virtual point cloud generation based on feature parameter modification

Taking the generation of virtual point clouds for girder components as an example, as shown in Figure 5. First, the primitive point set PS_{pr} is generated using the obtained size control nodes from the end sections. Then, parameters are adjusted for the initial plan extension, longitudinal extension equations, and span. (1) Modified planar equation $y = \hat{E}_P(x)$: In cases where the initial planar equation is a straight line, it can be adjusted to a circular arc equation. For bridges with original planar extensions in a curved form, different bridge characteristics can be created by altering the planar radius. (2) Modified longitudinal equation $z = \hat{E}_L(x)$: New longitudinal equations are formed by changing the longitudinal slope for girders with uniform cross-sections. Considering the correspondence between span and girder dimensions, longitudinal extensions are not applied separately to variable cross-section girders. (3) Modified span $\hat{S}$ and section size: New PCD is generated by altering the span. Simultaneously, dimensions should be adjusted to control node positions and refine cross-sectional sizes, ensuring that the height-to-span and height-to-width ratios of the main girder remain within reasonable limits, thereby achieving the optimal simulation of the real spatial features of the bridge.

Once the adjusted parameters are obtained, based on the end section primitive point set PS_{pr}, along with the modified planar equation, modified longitudinal equation, and modified span, a virtual bridge point cloud PC_{vi} is generated using the section replication method as per Equation (1), as depicted in Figure 5.

$$PC_{vi} = \sum_{i=0}^{St} \{x_i, y/z = \hat{E}_{\frac{P}{L}}(x_i)\}, x_i$$
$$= xinPS_{pr} + St \times i, i = 1, 2, \ldots, S/St \quad (1)$$

where St represents the section replication step size, a value determined based on the desired point cloud density. When performing planar extension transformation, use $y = \hat{E}_P(x)$, and when conducting longitudinal extension transformation, use $z = \hat{E}_L(x)$. If only span transformation is required, use the initial planar and longitudinal equations. S represents the bridge span, where S remains as the initial bridge span S_{in} if no span change is needed, and S is adjusted to the target span S_{tar} in the case of span modification.

Besides girder components, other structural elements can also be generated as virtual point clouds using similar methods. The deck, for instance, exhibits the same longitudinal extension characteristics as the girder beneath it, with the only difference being the cross-sectional shape. Although piers, main cables, suspenders, and stays all exhibit distinct spatial characteristics, virtual point clouds can generally be generated for these components using a similar workflow—starting from cross-sectional establishment, followed by extension equation fitting, spatial parameter adjustment, and cross-sectional replication. This is feasible because these elements are geometrically derived from the extension of a specific cross-sectional shape along a defined spatial path. For example, the main cable essentially consists of multiple circular cross-sections tightly aligned along a curved path.

3.2.3 | Real scanning state simulation of long-span bridge point cloud

Long-span bridges generally refer to bridges that span across rivers, seas, or mountainous areas, and they are primarily represented by suspension bridges and cable-stayed bridges. Due to their large spans, a significant number of scanning stations are required to ensure the completeness of PCD. The scanning process of a single long-span bridge often takes 2–3 days or even longer, and it may consume a

considerable amount of manpower and resources due to the complex scanning environment (H. W. Zhang et al., 2023). Therefore, the cost of acquiring a sufficient quantity of complete PCD for long-span bridges for model training sometimes far exceeds the efficiency improvement brought by learning-based bridge point cloud segmentation, depending on the scale and location of the bridge, the scanning equipment, and weather conditions.

For these long-span bridges, especially suspension bridges, the extended length in the plane can cause the laser's slip effect, resulting in inevitable and varying degrees of incompleteness in the point clouds of main girders and main cables. For a dataset used for semantic segmentation of bridge components, such point cloud incompleteness can provide non-authentic bridge component features to the network's learning process. Additionally, data incompleteness also leads to a reduction in the dataset size. Therefore, this study proposes a deficient point cloud generation approach to emulate the realistic conditions during the scanning of long-span bridges to the maximum extent. First, based on the virtual point cloud generation approach described in Section 2.2.2, the bridge's authentic dimensional information is still utilized to generate comprehensive PCD for components like main girders, bridge decks, main cables, suspenders and stays.

At the same time, considering the limitations of current ground-based laser scanning technology, even with meticulous station arrangements, scanned PCD of suspension bridges may exhibit some degree of incompleteness. Therefore, in this method, this study introduces a specific step for the part elimination of component point clouds, simulating the potential missing states of main cables, main girders, bridge decks, suspenders, and stays that might occur during real scans. For instance, the midspan part or the middle part of the girder and deck point cloud are eliminated, as shown in Figure 6a.i. Alternatively, point clouds that retained only the outer or inner half of the cross-sections for main cables, suspenders, and stays were generated as illustrated in Figure 6a.ii,iii. By including these artificial defects in the dataset, the model's robustness and ability to handle real-world PCD with missing components were improved, better simulating the challenges encountered in actual bridge scanning scenarios.

3.3 | Bridge components annotation

The types of bridge components are simple, but there are numerous types of bridges. If all different types of components from different types of bridges are classified separately in a dataset, it will inevitably result in a large number of target classes, making it more difficult for the network to learn and diminishing the practical value of the dataset. Therefore, a data annotation rule is proposed that goes beyond the types of bridges. As listed in Table 1, based on the uniqueness and similarities in the morphological structures of various bridge components, a universal, standardized semantic label for bridge components suitable for deep learning model training is created.

TABLE 1 Bridge component semantic labels.

Label	Girder	Deck	Pier
Component	Girder/crossbeam	Bridge deck	Pier/tower
Bridge type	G/S/C	G/S/C	G/S/C
Label	Main cable	Suspender	Stay
Component	Main cable	Suspender	Stay
Bridge type	S	S	C

Note: G, S, and C represent girder bridges, suspension bridges, and cable-stayed bridges, respectively.

Table 1 presents the categorization of bridge components in the dataset. In Table 1, G, S, and C represent girder bridges, suspension bridges, and cable-stayed bridges, respectively. The main girder and the potential bridge tower crossbeam components share a similar spatial configuration. They are both extended from a specific polygonal plane along the horizontal plane (or approximately) and, therefore, can be merged into a single label category. Main cable, suspender, and stay, although belonging to spatially extended components, are classified separately due to significant differences in their cross-sectional forms and modes of extension.

Both piers and towers are critical parts of the substructure and have similar spatial characteristics. Therefore, they can be combined into one category even though they belong to different bridge types. The bridge deck, as the only category of surface components, is specifically listed as a distinct class.

4 | STATISTICS FOR BrPCD

In the final BrPCD, a total of 98 bridges have been included (10 of them are obtained from real bridges, and 88 of them are virtual point clouds), covering various types of bridge PCD, and a total of 2827 bridge components commonly used as semantic segmentation targets in digital modeling. A full overview of the BrPCD is displayed in Figure 6b. BrPCD consists of 66 small and medium-span bridge PCD. This set includes four bridges with different spatial morphological features obtained from actual engineering projects, as well as two continuous girder bridges selected from publicly available datasets such as Lu's dataset (2019) to supplement bridge types that were

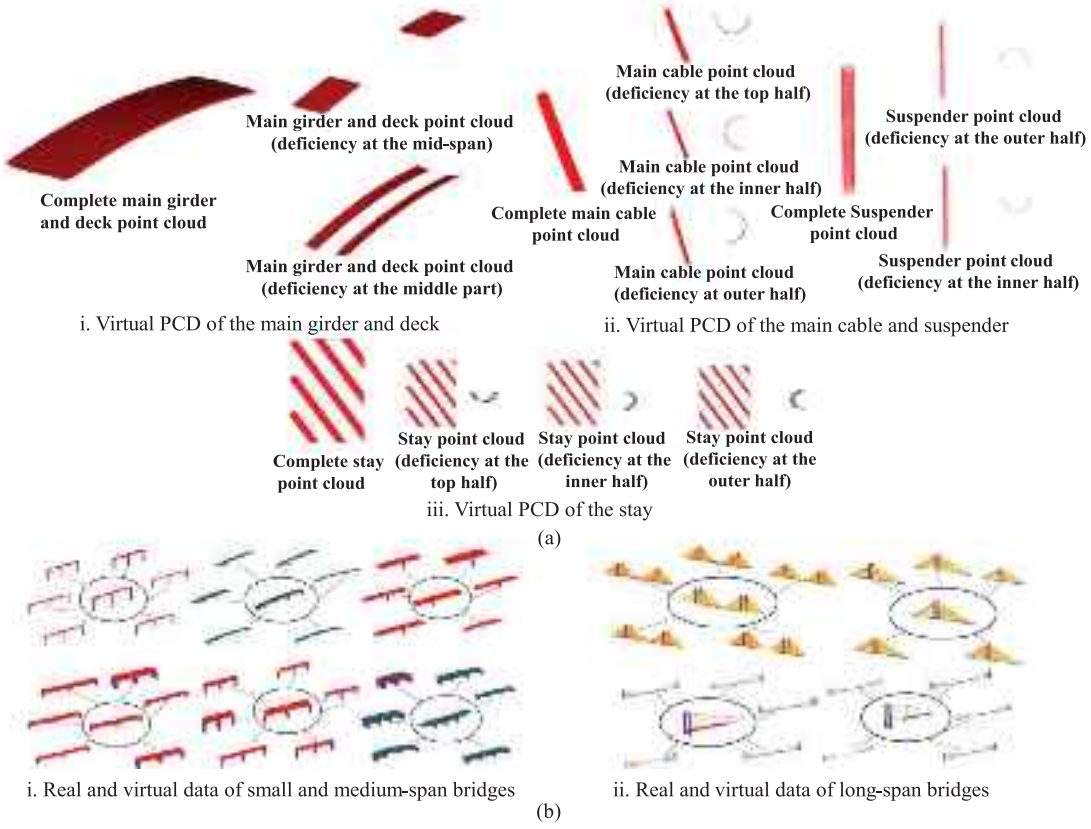

FIGURE 6 (a) Virtual PCD of different completeness and (b) panorama of BrPCD (virtual point clouds are partially displayed).

not covered in our scanning work. Among the 66 bridges, 60 bridges have been supplemented with virtual bridge PCD using the proposed data augmentation method for small and medium-span bridges. This method increases the number of different morphological features of small and medium-span bridges in the dataset by considering the longitudinal extension, planar extension, and span angles of the bridges.

Furthermore, the BrPCD includes four real captured point clouds of long-span bridges (two cable-stayed bridges and two suspension bridges) along with corresponding 28 virtual point clouds (32 long-span bridge point clouds in total). The virtual objects primarily include components such as main girders, bridge decks, main cables, suspenders, and stays, where PCD may suffer from severe incompleteness due to the large spans of the bridges. In the virtual point clouds, in addition to complete data generated based on actual bridge size information, this paper has also introduced artificially created defects. The summary of small and medium-span bridges and long-span bridges in the BrPCD is presented in Tables 2 and 3, respectively.

As presented in Table 2, the bridge types in the medium and small-span bridges category include continuous girder bridges and simply supported girder bridges, which have no significant differences in spatial features except for their differences in load characteristics. In terms of the longitudinal and planar extension modes of bridges, this study collected different combinations of curved and straight bridges, including inclined and horizontal straight bridges in the longitudinal direction. The type of main girder section is an important basis for distinguishing different bridge structures. In BrPCD, it includes several commonly used types of girders such as box girders, T-girders, and plate girders, which comprehensively cover the spatial features of main girders in medium and small-span bridges. To further enhance the diversity of structural features in the bridge PCD in the BrPCD and make the databank more adaptable to different deep learning networks, the data augmentation method proposed in Section 2.2 was used. Based on the original bridge point cloud's spatial morphology, the key parameters were modified to generate virtual bridge data with different extension modes and spans. This approach aimed to increase the diversity of bridge structure features in the databank.

Taking the example of "c-bridge1" from Table 2, the bridge is a continuous girder bridge with a curved planar profile characterized by a radius of 1500 m and a quadratic parabolic vertical curve. To diversify the databank without altering the span, additional bridge point clouds were generated. These included five point clouds with planar

TABLE 2 Summary of point cloud data (PCD) types for small and medium-span bridges.

	Real bridge PCD									
	Bridge description							Virtual bridge PCD		
Bridge span	**Bridge type**	**Longitudinal extension**	**Planar extension**	**Girder type**	**Girder number**	**Span type**	**Pier cross-section**	**Changed indicators**	**Bridge number**	**Component number**
Small and medium span	Continuous girder bridge (c-bridge1)	Curve	Curve	Box girder	Multi- girder	Medium span	Rectangle	Planar extension	5	25
								Span	5	25
	Continuous girder bridge (c-bridge2)	Horizontal straight line	Curve	Box girder	Single- girder	Small span	Rectangle/round	Planar extension	5	35
								Span	5	35
	Simple-supported girder bridge (s-bridge1)	Inclined straight line	Straight line	T-girder	Single- girder	Small span	Round	Longitudinal extension	5	55
								Span	5	55
	Continuous girder bridge (c-bridge3)	Horizontal straight line	Straight line	T-girder	Single- girder	Small span	Round	Planar extension	5	10
								Span	5	10
	Continuous girder bridge (c-bridge4)	Horizontal straight line	Straight line	Slab girder	Multi- girder	Small span	Round	Longitudinal extension	5	55
								Span	5	55
	Continuous girder bridge (c-bridge5)	Horizontal straight line	Curve	Slab girder	Multi- girder	Small span	Rectangle	Planar extension	5	30
								Span	5	30
Total bridge number: 66		**Total component number: 447**								

TABLE 3 Summary of PCD types for long-span bridges.

Bridge span	Real bridge PCD: Bridge description: Bridge type	Girder type	Span type	Virtual bridge PCD: Eliminated part	Bridge number	Component number
Long span	Suspension bridge (sus-bridge1)	Steel box girder	Long span (>1 km)	0(sus_f_bridge1)	1	140
				Main cable 50% (inside/outer side/upper side)	3	140
				Suspender 50% (inside/outer side)	2	140
				Main girder 50% (span/cross-section)	2	140
	Suspension bridge (sus-bridge2)	Steel box girder	Long span (>1 km)	0 (sus_f_bridge2)	1	188
				Main cable 50% (inside/outer side/upper side)	3	188
				Suspender 50% (inside/outer side)	2	188
				Main girder 50% (span/cross-section)	2	188
	Cable-stayed bridge (cs-bridge1)	Concrete box girder	Long span (<1 km)	0 (cs_f_bridge1)	1	119
				Stay 50% (inside/outer side/upper side)	3	119
				Main girder 50% (span/cross-section)	2	119
	Cable-stayed bridge (cs-bridge2)	Concrete box girder	Long span (<1 km)	0 (cs_f_bridge2)	1	237
				Stay 50% (inside/outer side/upper side)	3	237
				Deck 50% (span/cross-section)	2	237
Total bridge number: 32		**Total component number: 2380**				

curves having radii of 500, 1000, 2000, 2500, and 3000 m. Furthermore, five bridge point clouds with spans of 80, 90, 100, 140, and 160 m were created while maintaining the original planar curve. Figure 7a.i illustrates the "c-bridge1" and the corresponding virtual point clouds.

Similar procedures were applied to generate new PCD for the remaining five bridges with different structures. The transformation of bridge point cloud morphology follows real-world engineering practices. For instance, in the case of c-bridge4, which represents a single-pier highway overpass with a small span, the extension in the planar curve is not commonly observed. Therefore, the data augmentation process for c-bridge4 focused solely on adjusting the vertical curve to introduce variations in the inclination while maintaining the original planar straight extension. As depicted in Figure 7a.ii, K denotes the longitudinal slope of the bridge. Similar to s-bridge1 and c-bridge3, the data collection for c-bridge4 did not include the deck, consisting only of point clouds for the main girder and bridge pier. However, for the other bridges, in addition to the main girder and bridge pier, the PCD also includes the road surface as illustrated in Figure 7a.iii (using c-bridge2 as an example).

In the BrPCD, there are a total of 66 small and medium-span bridge PCD, which consist of both real bridge point clouds and virtual bridge point clouds. These bridges exhibit various spatial features, encompassing a total of 447 components with different spatial characteristics.

Table 3 first includes four real cable-supported bridges, consisting of two cable-stayed bridges (cs-bridge1, cs-bridge2) and two suspension bridges (sus-bridge1, sus-bridge2). cs-bridge1 is a single-tower cable-stayed bridge, and due to scanning limitations, the databank only includes the bridge deck, stays, and bridge tower. cs-bridge2 is a double-tower cable-stayed bridge, comprising the main girder, stays, and bridge towers. sus-bridge1 and sus-bridge2 are part of two cable-stayed bridges spanning over rivers and include the main girder, main cables, suspenders, and bridge towers.

In addition to real bridge PCD, the databank also includes 28 generated bridge PCD to provide sufficient and as realistic as possible samples for the learning process. The generated virtual point clouds comprise complete bridge point clouds, sus_f_bridge1, and sus_f_bridge2, created using the size parameters of sus_bridge1 and sus_bridge2 (the bridge towers are based on real data). To simulate the realistic states of existing long-span bridge PCD, various degrees of eliminations are introduced for components such as main cables, suspenders, and main girders on sus_f_bridge1 and sus_f_bridge2. In Table 3, the column "eliminated part" illustrates the positions and levels of point cloud elimination. "0" indicates generating

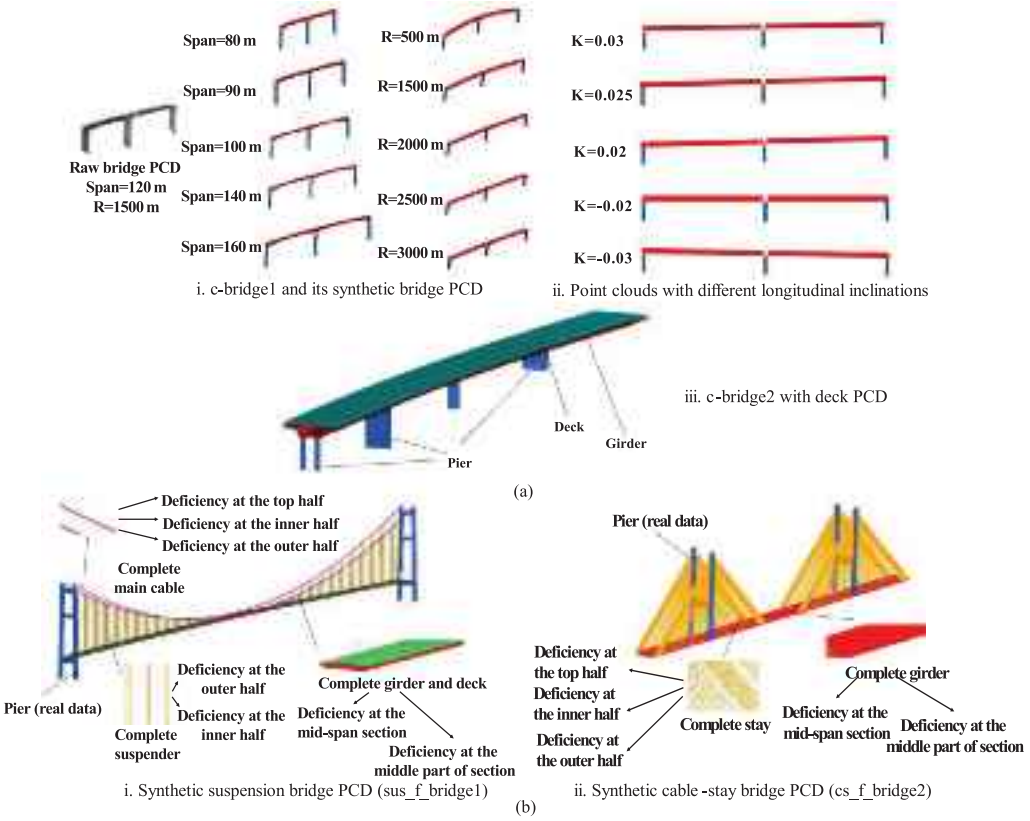

FIGURE 7 (a) Diversity in the databank and (b) virtual long-span bridge PCD.

complete virtual bridge point clouds, and "50% (inner, outer, upper)" indicates eliminating point clouds from the inner, outer, and upper sides of the main cables. The virtual suspension bridge point cloud is shown in Figure 7b.i. Similarly, the complete bridge point clouds cs_f_bridge1 and cs_f_bridge2 are generated based on the dimensional parameters of cs_bridge1 and cs_bridge2 (the towers are still the real data) and the eliminations are created for the stay components as shown in Figure 7b.ii.

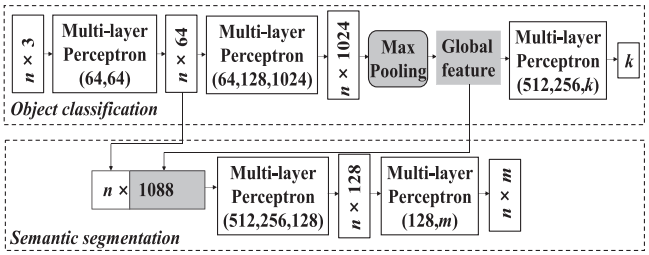

FIGURE 8 Architecture of the PointNet.

5 | VALIDATION AND EVALUATION OF BrPCD

5.1 | Segmentation network

In this study, the BrPCD contains various features of different types of bridges. To maximize the efficiency of learning PCD features, this paper conducted model validation using the widely adopted direct point cloud segmentation network, PointNet, on the BrPCD. PointNet is one of the earliest proposed networks designed to directly handle 3D PCD. It offers a novel approach to processing unordered point sets as network inputs without the need for converting point clouds into structured data. It effectively extracts point cloud features for shape classification and segmentation.

While many studies have developed more accurate point cloud segmentation networks based on PointNet, this paper chooses to use PointNet for its simplicity, efficiency, and suitability for validating large-scale bridge point cloud datasets. Furthermore, as one of the first direct point cloud segmentation networks, using PointNet for benchmark testing on the BrPCD provides a more intuitive reflection of its original performance in bridge point cloud segmentation tasks. Analyzing the network's prediction results can offer clearer insights and references for developing more specialized networks tailored for bridge point cloud segmentation tasks in the future.

The architecture of the PointNet is illustrated in Figure 8 (Qi et al., 2017). PointNet treats each point as an input and employs MLP to extract features from them separately. These features are then aggregated to obtain the global

TABLE 4 Mean accuracy (mAcc) and mean intersection over union (mIoU) of small and medium-span bridge.

	Group1 1/3 training set		Group2 2/3 training set		Group3 complete training set	
	Accuracy	mIoU	Accuracy	mIoU	Accuracy	mIoU
c-bridge1	0.855	0.823	0.931	0.877	**0.987**	**0.927**
c-bridge2	0.831	0.728	0.886	0.806	**0.912**	**0.836**
s-bridge1	0.820	0.799	0.917	0.827	**0.952**	**0.937**
c-bridge5	0.790	0.681	0.864	0.753	**0.900**	**0.797**

Note: The numbers highlighted with bold and underline indicate the best results.

features of the point cloud, ultimately resulting in the prediction of semantic labels for each point.

5.2 | Implementation details and evaluation indicators

The training was conducted using a GPU with 8GB memory, specifically an RTX 3070, and the PointNet model was implemented using the TensorFlow framework. The initial learning rate was set to 0.01, with a decay factor of 0.5. During training, the three-dimensional coordinates of each bridge point cloud were directly used as inputs. The batch size was set to 24, and each batch contained PCD with dimensions of 4096 × 3, where 4096 represents the number of points, and 3 represents the x, y, and z coordinates of each point. The training was performed for 50 epochs.

In our approach, the virtual PCD from the BrPCD (with one or two PCDs generated based on the bridge to be predicted included) and the real bridge point clouds (with the bridge PCDs to be predicted excluded) are used as the training set, while the bridge PCDs to be predicted are reserved for use as the test set. To avoid any cross-effects between labels of bridges with different sizes, the point cloud of small and medium-span bridges, cable-stayed bridges, and suspension bridges are divided into three separate parts for training and prediction. Simultaneously, the training set for each bridge type is divided into three groups with gradually increasing quantities, feeding 1/3, 2/3, and the entire training set point clouds into the network. Each group is set up by 50 epochs.

The parameters obtained from training are used for predicting the test set. The predicted results are assigned Red-Green-Blue (RGB) pixel values to visually observe the differences between the segmentation results and the ground truth. Additionally, two evaluation metrics, namely, mean accuracy (mAcc) and mean intersection over union (mIoU), were employed to further quantify the prediction performance. The calculation methods for these metrics are illustrated in Equations (2) and (3):

$$\text{Mean accuracy} = \sum_{i=1}^{N} \left(TP_i / \left(TP_i + FN_i\right)\right) / N \quad (2)$$

$$\text{Mean IoU} = \sum_{i=1}^{N} \left(TP_i / \left(TP_i + FP_i + FN_i\right)\right) / N \quad (3)$$

where N represents the number of labels. TP_i, FN_i, and FP_i correspond to the true positive (TP), false negative (FN), and false positive (FP) values for the ith label, respectively. TP signifies points that originally belong to a certain class and are correctly predicted as such. FN refers to points that actually belong to a certain class but are incorrectly predicted as belonging to other classes. FP indicates points that do not belong to a certain class but are wrongly predicted as belonging to that class.

5.3 | Segmentation results and evaluation

5.3.1 | Small and medium-span bridge

Table 4 lists the mAcc and mIoU results of predictions on the test set using parameters obtained from training with different groups of point clouds from small and medium-span bridges. From Table 4, it can be observed that with an increase in the number of training samples, the mAcc and mIoU for each bridge gradually improve. In the "Group3" column, trained with the entire training set, the segmentation accuracy for each bridge exceeds 0.9, with the highest approaching 0.99. Meanwhile, mIoU also maintains a high level. This illustrates that the inclusion of various spatial features of different bridges in BrPCD enhances the adaptability of the network parameters for bridge semantic segmentation tasks.

Table 5 presents the IoU for each label in the test set bridges. The "–" symbol indicates the absence of

TABLE 5 Label IoU of small and medium-span bridge.

	Girder	Deck	Pier
c-bridge1	0.986	–	0.867
c-bridge2	0.922	0.754	0.833
s-bridge1	0.950	–	0.924
c-bridge5	0.811	0.790	0.791

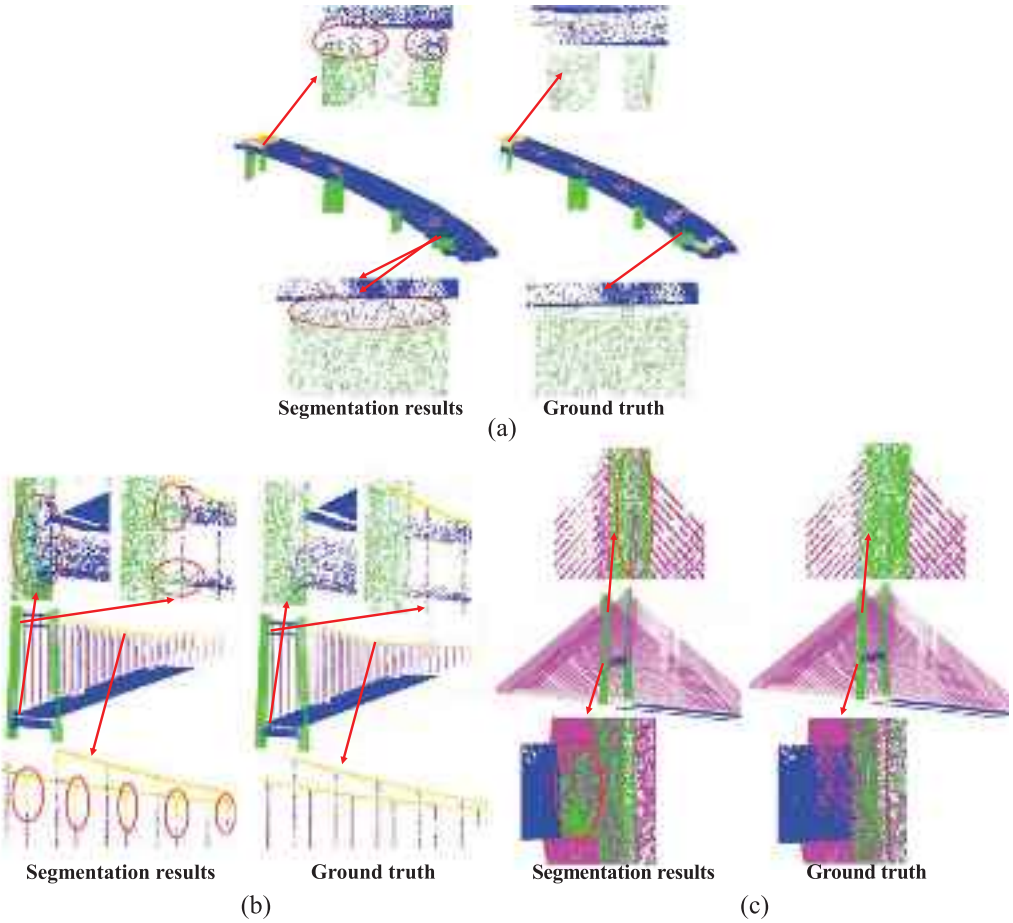

FIGURE 9 Comparison of ground truth and segmentation results for (a) small and medium-span bridge, (b) suspension bridge, (c) cable-stayed bridge. (Incorrect predictions are marked with red ovals.

components with that label in the respective bridge. In Table 5, it can be observed that the IoU values for various labels in small and medium-span bridges are relatively high. Consequently, the corresponding mIoU values in Table 4 also maintain a high level. In comparison to other studies utilizing PointNet for bridge segmentation, this research achieves higher accuracy in bridge segmentation due to BrPCD's larger dataset and richer spatial features. However, the IoU for the pier label is lower than that of other labels.

Comparative analysis of ground truth and prediction results through RGB images. From Figure 9a, it can be observed that PointNet generally achieves good segmentation accuracy for small and medium-span bridges. However, there are still noticeable errors in the prediction of the connection between the pier and the main girder, primarily manifested by certain points on the top of the pier near the main girder being misclassified as points belonging to the main girder. This phenomenon may be attributed to the PointNet's insufficient capacity for extracting local features and its lack of consideration for the interrelations between individual points. Since the connection area between the pier and the girder represents a localized region with significant spatial feature variations, PointNet struggles to accurately differentiate the features of these two labels.

5.3.2 | Long-span bridge

Table 6 displays the mAcc and mIoU results for long-span bridges. Similar to small and medium-span bridges, the mAcc and mIoU for long-span bridges also improve with an increase in the number of bridge samples in the training set, reaching highs of approximately 0.97 and 0.88, respectively. This demonstrates the effectiveness of the dataset for the automated segmentation of this type of bridge.

However, as evident from the IoU values for each label in Table 7, similar to small and medium-span bridges, in suspension bridges, the IoU value for the pier label (bridge tower and tower crossbeam) is relatively lower compared to other labels. In the case of cable-stayed bridges, this phenomenon is more pronounced, with the IoU value for the pier label dropping even below 0.7.

TABLE 6 mAcc and mIoU of long-span bridge.

	Group1 1/3 training set		Group2 2/3 training set		Group3 complete training set	
	Accuracy	mIoU	Accuracy	mIoU	Accuracy	mIoU
sus-bridge1	0.855	0.736	0.918	0.823	**0.966**	**0.879**
sus-bridge2	0.827	0.703	0.906	0.812	**0.928**	**0.865**
cs-bridge1	0.883	0.681	0.921	0.768	**0.943**	**0.815**
cs-bridge2	0.839	0.701	0.879	0.753	**0.906**	**0.788**

Note: The numbers highlighted with bold and underline indicate the best results.

TABLE 7 Label IoU of long-span bridge.

	Girder	Pier	Deck	Main cable	Suspender	Stay
sus-bridge1	0.976	0.834	—	0.871	0.835	—
sus-bridge2	0.935	0.913	0.782	0.833	0.861	—
cs-bridge1	0.926	0.635	—	—	—	0.883
cs-bridge2	0.823	0.717	0.735	—	—	0.875

Figure 9b,c, respectively, show the visualization results of predicted and ground truth values for the point clouds of suspension bridges and cable-stayed bridges. It can be observed that there are prediction errors at the connection between the tower and crossbeam in both types of bridge point clouds. Especially, in the suspension bridge, a small number of points on the suspender near the main cable are mistakenly predicted as part of the main cable. In cable-stayed bridges, some points near the cable tower are misclassified as cables. This is also the reason why the IoU values for the pier label in cable-stayed bridges are lower than those in suspension bridges as shown in Table 7. The limited capacity of PointNet for learning local features, combined with its treatment of each point as an independent entity, hampers its ability to effectively capture and model the relationships between points, particularly in complex areas such as the connections between the bridge tower and the transverse girder or the bridge tower and the main cable. This limitation ultimately results in ambiguous boundary predictions. Clear structural boundaries are crucial in modal analysis (Li et al., 2017; Pezeshki, Pavlou, et al., 2023).

When all bridge point clouds were used for training, the visualized results indicated that the prediction accuracy at component connections remained unsatisfactory for small to large-span bridges. This issue primarily stems from inherent limitations in the PointNet as previously analyzed. However, these results also lead to a discussion on whether the sample size in the dataset is sufficient. In theory, the number of bridges included in a bridge point cloud dataset is limitless, especially when considering the proposed data augmentation method. However, an infinite increase in sample size does not necessarily lead to a continuous improvement in prediction results. Enhancing segmentation precision in specific local details relies on a higher level of feature learning capability within the network. Therefore, the number of bridges included in the dataset should be determined by the specific task at hand, such as the number of target bridges and the complexity of the target components.

6 | CONCLUSION

To address the gap in available bridge point cloud datasets for model training and to provide a foundational and universal dataset for comparative evaluation of prediction performance across various deep learning networks, this research establishes the BrPCD, a universal multi-type bridge point cloud databank including 2827 individual bridge components. Features of BrPCD are drawn as follows:

1. Dataset size. The BrPCD contains various bridges with diverse spatial features, including six real small and medium-span bridges and four real long-span bridges (suspension bridges and cable-stayed bridges), 88 virtual bridge point clouds, and 2827 individual bridge components.
2. Dataset augmentation solution. A data augmentation method is developed for BrPCD establishment based on feature parameter variation. This method relies on feature extraction from existing point clouds and blueprints and manufacturing feature modifications to achieve data augmentation. Feature parameters are modified from three angles: planar extension, longitudinal extension, and span. Especially, for long-span bridges, a part elimination-based method is proposed to simulate the point cloud features of bridge

components as closely as possible to those obtained through real scanning.
3. Dataset annotation. A new labeling technique for bridge point clouds that is based on the traits and commonalities of components is also proposed for bridge point clouds in this article. By using this labeling technique, deep learning networks' output dimension can be decreased while still allowing BrPCD to adapt to a greater variety of point cloud segmentation tasks for various bridge kinds.

To evaluate the feasibility and accuracy of BrPCD, the PointNet model is employed for training and prediction. Several results can be highlighted as follows:

1. The component segmentation is performed on three data subsets separately, which are categorized by the bridge types considering the component similarity, that is, small- and medium-span bridges, cable-stayed bridges, and suspension bridges separately. From the segmentation accuracy, it can be observed that training based on BrPCD enables accurate component segmentation for the three different types of bridges mentioned above.
2. In terms of medium and small-span bridges' segmentation, the overall accuracy can reach over 90%. However, based on the IoU values for pier labels (approximately 83% to 93%) and the visual results of segmentation, the segmentation precision of the pier-main girder junction should be prioritized as an enhancement target in future endeavors for this category of bridge component segmentation.
3. Concerning the segmentation of long-span bridges, the overall segmentation accuracy can reach 95% or higher. However, the IoU values for pier labels are relatively low (around 60% for the two cable-stayed bridges). In combination with the visual segmentation results, some points at the connections between different components are inaccurately predicted. While the prediction errors at some of these connection points are relatively small (the IoU values for main cables, suspenders, girders, and stay labels remain at approximately 90%), these inaccuracies can impact the process of bridge informatization modeling. Therefore, improving the accuracy of these connection points is a key focus for future research in segmentation models.

In summary, the establishment of BrPCD addresses the deficiency in a comprehensive multi-type bridge point cloud dataset, providing researchers with parameters applicable to bridge point cloud segmentation, including both small- to medium-span bridges and long-span bridges. It serves as a unified platform for comparing and analyzing the predictive performance of various point cloud segmentation networks. While utilizing BrPCD for model training enhances the accuracy of bridge segmentation, challenges persist in addressing the lower accuracy of connections between specific bridge components, necessitating improvements from a model enhancement perspective.

ACKNOWLEDGMENTS

The financial support for this work from the National Natural Science Foundation of China (Project Nos. 52378135 and 52108118) are gratefully acknowledged. The opinions and statements do not necessarily represent those of the sponsors.

DATA AVAILABILITY STATEMENT

The BrPCD can be downloaded by the following link https://github.com/wxiong12/SEU-Digital-Bridge.

REFERENCES

Armeni, I., Sener, O, Zamir, A. R., Jiang, H., Brilakis, I., & Fischer, M. (2016). 3D semantic parsing of large-scale indoor spaces. *2016 IEEE Conference on Computer Vision and Pattern Recognition*, Las Vegas, NV (pp. 1534–1543). https://doi.org/10.1109/cvpr.2016.170

Belsky, M., Sacks, R., & Brilakis, I. (2016). Semantic enrichment for building information modeling. *Computer-Aided Civil and Infrastructure Engineering*, *31*(4), 261–274. https://doi.org/10.1111/mice.12128

Boulch, A., Guerry, J., Le Saux, B., & Audebert, N. (2018). SnapNet: 3D point cloud semantic labeling with 2D deep segmentation networks. *Computers & Graphics-Uk*, *71*, 189–198. https://doi.org/10.1016/j.cag.2017.11.010

Chen, J., & Cho, Y. K. (2022). CrackEmbed: Point feature embedding for crack segmentation from disaster site point clouds with anomaly detection. *Advanced Engineering Informatics*, *52*, e101550. https://doi.org/10.1016/j.aei.2022.101550

Gaidon, A., Wang, Q., Cabon, Y., & Vig, E. (2016). Virtual worlds as proxy for multi-object tracking analysis. *2016 IEEE Conference on Computer Vision and Pattern Recognition*, Las Vegas, NV (pp. 4340–4349). https://doi.org/10.1109/cvpr.2016.470

Gori, M., Monfardini, G., & Scarselli, F. (2005). A new model for learning in graph domains. *Proceedings of the International Joint Conference on Neural Networks (IJCNN)*, Montréal, Québec, Canada (pp. 729–734). https://doi.org/10.1109/ijcnn.2005.1555942

Hackel, T., Wegner, J. D., Savinov, N., Ladicky, L., Schindler, K., & Pollefeys, M. (2018). Large-scale supervised learning for 3D point cloud labeling: Semantic3d.Net. *Photogrammetric Engineering and Remote Sensing*, *84*(5), 297–308. https://doi.org/10.14358/pers.84.5.297

Himmelsbach, M., Hundelshausen, F. v., & Wuensche, H.-J. (2010). Fast segmentation of 3D Point clouds for ground vehicles. *2010 IEEE Intelligent Vehicles Symposium*, La Jolla, CA (pp. 560–565). https://doi.org/10.1109/ivs.2010.5548059

Hinton, G. E., & Salakhutdinov, R. R. (2006). Reducing the dimensionality of data with neural networks. *Science*, *313*(5786), 504–507. https://doi.org/10.1126/science.1127647

Hu, Q., Yang, B., Xie, L., Rosa, S., Guo, Y., Wang, Z., Trigoni, N., & Markham, A. (2020). RandLA-Net: Efficient semantic segmentation of large-scale point clouds. *2020 IEEE/CVF Conference on Computer Vision and Pattern Recognition*, Seattle, WA. https://doi.org/10.1109/cvpr42600.2020.01112

Javadinasab Hormozabad, S., Gutierrez Soto, M., & Adeli, H. (2021). Integrating structural control, health monitoring, and energy harvesting for smart cities. *Expert Systems*, *38*(8), e12845. https://doi.org/10.1111/exsy.12845

Jing, Y., Sheil, B., & Acikgoz, S. (2022). Segmentation of large-scale masonry arch bridge point clouds with a synthetic simulator and the BridgeNet neural network. *Automation in Construction*, *142*, e104459. https://doi.org/10.1016/j.autcon.2022.104459

Jing, Y., Sheil, B., & Acikgoz, S. (2024). A lightweight Transformer-based neural network for large-scale masonry arch bridge point cloud segmentation. *Computer-Aided Civil and Infrastructure Engineering*, *39*(16), 2427–2438. https://doi.org/10.1111/mice.13201

Joseph-Rivlin, M., Zvirin, A., & Kimmel, R. (2019). Momenet: Flavor the moments in learning to classify shapes. *2019 IEEE/CVF International Conference on Computer Vision Workshops (ICCVW)*, Seoul, Korea (pp. 4085–4094).

Kalogerakis, E., Hertzmann, A., & Singh, K. (2010). Learning 3D mesh segmentation and labeling. *ACM Transactions on Graphics*, *29*(4), e1778839. https://doi.org/10.1145/1778765.1778839

Kim, H., & Kim, C. (2020). Deep-learning-based classification of point clouds for bridge inspection. *Remote Sensing*, *12*(22), 3757. https://doi.org/10.3390/rs12223757

Kim, H., Yoon, J., & Sim, S.-H. (2020). Automated bridge component recognition from point clouds using deep learning. *Structural Control & Health Monitoring*, *27*(9), e2591. https://doi.org/10.1002/stc.2591

Kipf, T. N., & Welling, M. (2017). Semi-supervised classification with graph convolutional networks. *5th International Conference on Learning Representations, ICLR 2017*, Toulon, France. https://doi.org/10.48550/arXiv.1609.02907

Laefer, D. F., & Truong-Hong, L. (2017). Toward automatic generation of 3D steel structures for building information modelling. *Automation in Construction*, *74*, 66–77. https://doi.org/10.1016/j.autcon.2016.11.011

Lecun, Y., Bengio, Y., & Hinton, G. (2015). Deep learning. *Nature*, *521*(7553), 436–444. https://doi.org/10.1038/nature14539

Lee, J. S., Park, J., & Ryu, Y.-M. (2021). Semantic segmentation of bridge components based on hierarchical point cloud model. *Automation in Construction*, *2021*, 130. https://doi.org/10.1016/j.autcon.2021.103847

Li, Z., Park, H. S., & Adeli, H. (2017). New method for modal identification and health monitoring of superhighrise building structures using discretized synchrosqueezed wavelet and hilbert transforms. *The Structural Design of Tall and Special Buildings*, *26*(3), e1312. https://doi.org/10.1002/tal.1312

Liang, H., Yeoh, J. K. W., & Chua, D. K. H. (2024). Material augmented semantic segmentation of point clouds for building elements. *Computer-Aided Civil and Infrastructure Engineering*, *39*(15), 2312–2329. https://doi.org/10.1111/mice.13198

Liang, Q., Wang, Y., Nie, W., & Li, Q. (2020). MVCLN: Multi-view convolutional LSTM network for cross-media 3D shape recognition. *IEEE Access*, *8*, 139792–139802. https://doi.org/10.1109/access.2020.3012692

Lu, R., Brilakis, I., & Middleton, C. R. (2019). Detection of structural components in point clouds of existing RC bridges. *Computer-Aided Civil and Infrastructure Engineering*, *34*(3), 191–212. https://doi.org/10.1111/mice.12407

Ma, L., Sacks, R., Kattel, U., & Bloch, T. (2018). 3D object classification using geometric features and pairwise relationships. *Computer-Aided Civil and Infrastructure Engineering*, *33*(2), 152–164. https://doi.org/10.1111/mice.12336

Martens, J., Blut, T., & Blankenbach, J. (2023). Cross domain matching for semantic point cloud segmentation based on image segmentation and geometric reasoning. *Advanced Engineering Informatics*, *57*, e102076. https://doi.org/10.1016/j.aei.2023.102076

Martins, G. B., Papa, J. P., & Adeli, H. (2020). Deep learning techniques for recommender systems based on collaborative filtering. *Expert Systems*, *37*(6), e12647. https://doi.org/10.1111/exsy.12647

Matono, G., & Nishio, M. (2024). Component-level point cloud completion of bridge structures using deep learning. *Computer-Aided Civil and Infrastructure Engineering*, *39*(17), 2581–2595. https://doi.org/10.1111/mice.13218

Mian, A. S., Bennamoun, M., & Owens, R. (2006). Three-dimensional model-based object recognition and segmentation in cluttered scenes. *IEEE Transactions on Pattern Analysis and Machine Intelligence*, *28*(10), 1584–1601. https://doi.org/10.1109/tpami.2006.213

Mo, K., Zhu, S., Chang, A. X., Yi, L., Tripathi, S., Guibas, L. J., & Su, H. (2019). PartNet: A large-scale benchmark for fine-grained and hierarchical part-level 3D Object understanding. *2019 IEEE/CVF Conference on Computer Vision and Pattern Recognition*, Long Beach, CA (pp. 909–918). https://doi.org/10.1109/cvpr.2019.00100

Noichl, F., Collins, F. C., Braun, A., & Borrmann, A. (2024). Enhancing point cloud semantic segmentation in the data-scarce domain of industrial plants through synthetic data. *Computer-Aided Civil and Infrastructure Engineering*, *39*(10), 1530–1549. https://doi.org/10.1111/mice.13153

Pan, X., Yang, T. Y., Xiao, Y., Yao, H., & Adeli, H. (2023). Vision-based real-time structural vibration measurement through deep-learning-based detection and tracking methods. *Engineering Structures*, *281*, e115676. https://doi.org/10.1016/j.engstruct.2023.115676

Perez-Ramirez, C. A., Amezquita-Sanchez, J. P., Valtierra-Rodriguez, M., Adeli, H., Dominguez-Gonzalez, A., & Romero-Troncoso, R. J. (2019). Recurrent neural network model with Bayesian training and mutual information for response prediction of large buildings. *Engineering Structures*, *178*, 603–615. https://doi.org/10.1016/j.engstruct.2018.10.065

Pezeshki, H., Adeli, H., Pavlou, D., & Siriwardane, S. C. (2023). State of the art in structural health monitoring of offshore and marine structures. *Proceedings of the Institution of Civil Engineers—Maritime Engineering*, *176*(2), 89–108. https://doi.org/10.1680/jmaen.2022.027

Pezeshki, H., Pavlou, D., Adeli, H., & Siriwardane, S. C. (2023). Modal analysis of offshore wind turbine structures: An analytical solution. *ASME Journal of Offshore Mechanics and Arctic Engineering*, *145*(1), e010907. https://doi.org/10.1115/1.4055402

Qi, C. R., Su, H., Kaichun, M., & Guibas, L. J. (2017). PointNet: Deep learning on point sets for 3D classification and segmentation. *30th IEEE Conference on Computer Vision and Pattern Recognition*, Honolulu, HI (pp. 77–85). https://doi.org/10.1109/cvpr.2017.16

Qi, C. R., Yi, L., Su, H., & Guibas, L. J. (2017). PointNet++: Deep hierarchical feature learning on point sets in a metric space. *Advances in Neural Information Processing Systems 30*, Long Beach, CA.

Rafiei, M. H., & Adeli, H. (2017). A novel machine learning based algorithm to detect damage in highrise building structures. *The Structural Design of Tall and Special Buildings*, *26*(18), e1400. https://doi.org/10.1002/tal.1400

Riveiro, B., Dejong, M. J., & Conde, B. (2016). Automated processing of large point clouds for structural health monitoring of masonry arch bridges. *Automation in Construction*, *72*, 258–268. https://doi.org/10.1016/j.autcon.2016.02.009

Scarselli, F., Gori, M., Ah Chung Tsoi, Hagenbuchner, M., & Monfardini, G. (2009). The graph neural network model. *IEEE Transactions on Neural Networks*, *20*(1), 61–80. https://doi.org/10.1109/tnn.2008.2005605

Simonovsky, M., & Komodakis, N. (2017). Dynamic edge-conditioned filters in convolutional neural networks on graphs. *30th IEEE Conference on Computer Vision and Pattern Recognition*, Honolulu, HI (pp. 29–38). https://doi.org/10.1109/cvpr.2017.11

Song, X., Wang, P., Zhou, D., Zhu, R., Guan, C., & Dai, Y. (2019). ApolloCar3D: A large 3D car instance understanding benchmark for autonomous driving. *2019 IEEE/CVF Conference on Computer Vision and Pattern Recognition*, Long Beach, CA (pp. 5447–5457). https://doi.org/10.1109/cvpr.2019.00560

Wang, L., Huang, Y., Shan, J., & He, L. (2018). MSNet: Multi-scale convolutional network for point cloud classification. *Remote Sensing*, *10*(4), 612. https://doi.org/10.3390/rs10040612

Wang, Y., Sun, Y., Liu, Z., Sarma, S. E., Bronstein, M. M., & Solomon, J. M. (2019). Dynamic graph CNN for learning on point clouds. *ACM Transactions on Graphics*, *38*(5), e3326362. https://doi.org/10.1145/3326362

Wu, Z., Song, S., Khosla, A., Yu, F., Zhang, L., & Tang, X. (2015). 3D ShapeNets: A deep representation for volumetric shapes. *2015 IEEE Conference on Computer Vision And Pattern Recognition (CVPR 2015)*, Boston, MA (pp. 1912–1920). https://doi.org/10.1109/cvpr.2015.7298801

Xia, T., Yang, J., & Chen, L. (2022). Automated semantic segmentation of bridge point cloud based on local descriptor and machine learning. *Automation in Construction*, *133*, 103992. https://doi.org/10.1016/j.autcon.2021.103992

Xu, Y., Hoegner, L., Tuttas, S., & Stilla, U. (2018). A voxel- and graph-based strategy for segmenting man-made infrastructures using perceptual grouping laws: Comparison and evaluation. *Photogrammetric Engineering and Remote Sensing*, *84*(6), 377–391. https://doi.org/10.14358/pers.84.6.377

Yang, J., Zhang, Q., Ni, B., Li, L., Liu, J., & Zhou, M. (2019). Modeling point clouds with self-attention and gumbel subset sampling. *2019 IEEE/CVF Conference on Computer Vision and Pattern Recognition*, Long Beach, CA (pp. 3318–3327). https://doi.org/10.1109/cvpr.2019.00344

Yang, X., Del Rey Castillo, E., Zou, Y., Wotherspoon, L., & Tan, Y. (2022). Automated semantic segmentation of bridge components from large-scale point clouds using a weighted superpoint graph. *Automation in Construction*, *142*, 104519.

Yi, L., Shao, L., Savva, M., Huang, H., Zhou, Y., Wang, Q., Graham, B., Engelcke, M., Klokov, R., Lempitsky, V., Gan, Y., Wang, P., Liu, K., Yu, F., Shui, P., Hu, B., Zhang, Y., Li, Y., Bu, R., … Guibas, L. (2017). *Large-scale 3D shape reconstruction and segmentation from ShapeNet Core55*. Arxiv. https://doi.org/10.48550/arXiv.1710.06104

Zhang, G., Vela, P. A., Karasev, P., & Brilakis, I. (2015). A sparsity-inducing optimization-based algorithm for planar patches extraction from noisy point-cloud data. *Computer-aided Civil and infrastructure Engineering*, *30*(2), 85–102. https://doi.org/10.1111/mice.12063

Zhang, H. W., Zhu, Y., Xiong, W., & Cai, C. S. (2023). Point cloud registration methods for long-span bridge spatial deformation monitoring using terrestrial laser scanning. *Structural Control & Health Monitoring*, *2023*, e2629418, https://doi.org/10.1155/2023/2629418

Zhang, J., Zhao, X., Chen, Z., & Lu, Z. (2019). A Review of deep learning-based semantic segmentation for point cloud. *IEEE Access*, *7*, 179118–179133. https://doi.org/10.1109/access.2019.2958671

Zhang, R., Li, G., Wunderlich, T., & Wang, L. (2021). A survey on deep learning-based precise boundary recovery of semantic segmentation for images and point clouds. *International Journal of Applied Earth Observation and Geoinformation*, *102*, e102411. https://doi.org/10.1016/j.jag.2021.102411

Zhang, Y., Xia, B., & Taylor, S. (2024). High-resolution 3-D geometry updating of digital functional models using point cloud processing and surface cut. *Computer-Aided Civil and Infrastructure Engineering*, *39*(1), 3–19. https://doi.org/10.1111/mice.13076

Zhang, Z., Liang, D., Huang, H., & Sun, L. (2024). Virtual trial assembly of large steel members with bolted connections based on multi-scale point cloud fusion. *Computer-Aided Civil and Infrastructure Engineering*, *39*(17), 2619–2641. https://doi.org/10.1111/mice.13210

Zhao, H., Jiang, L., Fu, C.-W., & Jia, J. (2019). PointWeb: Enhancing local neighborhood features for point cloud processing. *2019 IEEE/CVF Conference on Computer Vision and Pattern Recognition*, Long Beach, CA (pp. 5550–5558). https://doi.org/10.1109/cvpr.2019.00571

How to cite this article: Zhang, H., Zhu, Y., Xiong, W., & Cai, C. S. (2025). A bridge point cloud databank for digital bridge understanding. *Computer-Aided Civil and Infrastructure Engineering*, *40*, 1253–1271. https://doi.org/10.1111/mice.13384